

Light emission induced by a scanning tunnel microscope from a doubly layered substrate

Katsuki Amemiya

National Institute for Materials Science, 1-2-1 Sengen, Tsukuba, Ibaraki 305-0047, Japan

(Received 11 September 2002; published 13 February 2003)

Photon emission induced by a scanning tunneling microscope is studied theoretically when a substrate is covered with a layer of finite thickness. We formulate the calculation method of the radiated power including the retardation effect. Calculation of a metal film on a dielectric substrate indicates that the optimal thickness for the effective photon emission exists for the silver film. The effect of a dielectric film on a metal substrate is also investigated and it is found that the radiated power from the STM is enhanced strongly by putting the dielectric layer on the substrate.

DOI: 10.1103/PhysRevB.67.075409

PACS number(s): 68.37.Ef, 42.25.Bs, 73.20.Mf, 78.20.Bh

I. INTRODUCTION

More than a decade ago the scanning tunneling microscope (STM) induced photon emission was first observed,¹ and the theoretical calculations performed soon later have shown very good agreement with the experimental results.^{2,3} Its origin is considered as the excitation of the localized surface plasmon induced in the tip-sample gap region by the STM current, and its decay into the radiation field. Since then, it has been applied to various tip and sample materials. It depends not only on tip and substrate materials, but also on tip shapes and sample surface condition. Because of the sensitivity of the tip-sample condition, this may present variety of ways of surface analysis. Moreover, there is a possibility to use it as a nanoscale light emission mechanism.

A number of theoretical analyses have been performed, and many of them were based on the electromagnetic field calculation induced by the point current source in the tip-sample geometry. Earliest attempts were based on the system of a sphere above a plane.^{2,4,5} They are nonretarded calculations, but later Johansson included the retarded effect in the theory.⁶ Moreover, theoretical works have also demonstrated that the sample size or tip shape influences the photon emission spectra considerably.⁷⁻¹⁰ A sample having the corrugated surface has also been discussed.¹¹

When a sample has the flat surface, however, the effect of the substrate thickness on the light emission is rarely paid attention to. So far, semi-infinite substrates were assumed in most theoretical approaches. This assumption is well validated in a usual experimental situation where the thickness of the metal substrate is much larger than the skin depth in the optical range. However, there should be some change when the metal thickness becomes smaller and comparable to the skin depth, and the spectrum may be pretty affected by the metal thickness.

Another interest is a dielectric film on a metal substrate. Experiments on the photon emission STM (PESTM) using substrates covered with organic molecules have been performed from just after the discovery of PESTM,¹²⁻¹⁵ and it is expected as an observation tool for physical and chemical states of molecular layers on substrates. Although interests of some of them may be in the luminescence from the individual molecules in the STM configuration, it is very hard to identify the location of the single molecules when their distribution is sparse. Consequently, the molecules were cover-

ing most of the area. Therefore, this system may act similar to a metal substrate covered with an organic thin film. Though it may be a rough estimation to approximate those molecular layers as a dielectric film, we think some information can be obtained by this calculation.

In order to treat both of these cases, that is, a metal film on a dielectric substrate and a dielectric film on a metal substrate, we formulate the calculation method for a doubly layered substrate. As this calculation gives an exact solution of the Maxwell equation, the retardation effect is fully taken into account. By using this method we will show how the layer of finite thickness on the substrate surface has an effect on the light emission from the STM.

II. MODEL

As described in Refs. 2 and 4, calculation of light emission from STM can be divided into two parts; one is the calculation of the electromagnetic field induced by the *classical* current source, and the other is the calculation of the power spectrum of the current fluctuations. We also use this method to compute the radiated power induced by the STM current. For simplicity, we use a model which has been often employed; that is, the STM tip is replaced with a sphere having radius of a . The origin of the coordinate system is the center of the sphere, and the z axis is taken as normal to the substrate surface (Fig. 1). It is assumed that the current source \mathbf{j} exists just below the sphere, $\mathbf{r}_0 = (0, 0, -a - 0)$, and the electric field \mathbf{E} in the far region should be calculated. The reciprocity theorem is used to calculate the far field induced by the source \mathbf{j} .¹⁶ By this theorem, the electric field can be calculated by exchanging the source and observation point, and the problem is reduced to computing the z component of the electric field \mathbf{E}_p below the sphere when the point current source $\mathbf{j}_p(\mathbf{r}) = j_p \hat{\theta}' \delta^3(\mathbf{r} - \mathbf{r}_p)$ is far away from the tip-sample gap (Fig. 1), where θ' is the angle between the z axis and $\mathbf{r}_p - \mathbf{r}_0$, and $\hat{\theta}'$ is the unit vector which is perpendicular to $\mathbf{r}_p - \mathbf{r}_0$ and is on the x - z plane. Since the source is far enough from the system, the electric field in the gap region is obtained by using a calculated result of the electric field \mathbf{E}' when the plane wave of the p polarization is incident on the system.⁴

For the calculation of the electromagnetic field \mathbf{E}' in the system of the sphere above the substrate, we employed the

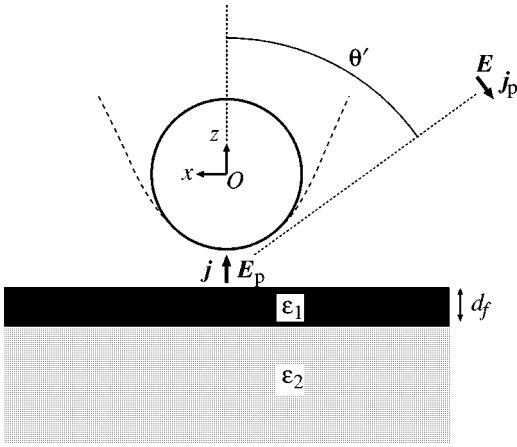


FIG. 1. Model for calculation of the light emission STM using the reciprocity theorem.

vector spherical wave expansion method used by Takemori and co-workers.¹⁷ In the polar coordinate system, the vector spherical waves needed for the analysis of electromagnetic fields are the transversal ones, which are called M and N waves following the expression used by Stratton.¹⁸ The concrete forms of M and N waves in polar coordinates are

$$\epsilon_L^M(f, k, \mathbf{r}) = \begin{pmatrix} 0 \\ -\frac{1}{\sin \theta} \frac{\partial}{\partial \phi} \\ \frac{\partial}{\partial \theta} \end{pmatrix} f_l(kr) Y_L(\hat{\mathbf{r}}), \quad (1)$$

$$\epsilon_L^N(f, k, \mathbf{r}) = \begin{pmatrix} -l(l+1)f_l(kr) \\ -\left[\frac{\partial}{\partial r} r f_l(kr)\right] \frac{\partial}{\partial \theta} \\ -\left[\frac{\partial}{\partial r} r f_l(kr)\right] \frac{1}{\sin \theta} \frac{\partial}{\partial \phi} \end{pmatrix} \frac{1}{kr} Y_L(\hat{\mathbf{r}}), \quad (2)$$

where f_l is the spherical Bessel function j_l , the spherical Neumann function n_l , or the spherical Hankel function of the first kind $h_l^{(1)}$. $k = \omega/c$, ω is the frequency of the field and c is the speed of light. $Y_L(\hat{\mathbf{r}})$ is the spherical harmonic of angular momentum $L = (l, m)$.¹⁹ The plane wave can be expanded by the vector spherical waves as

$$\mathbf{E}^0 e^{i\mathbf{k} \cdot \mathbf{r}} = \sum_{\beta=M,N} \sum_L \epsilon_L^\beta(j, k, \mathbf{r}) \alpha_L^\beta(0), \quad (3)$$

where the amplitude $\alpha_L^\beta(0)$ is

$$\alpha_L^\beta(0) = \frac{1}{l(l+1)} \sum_{j=x,y,z} \sum_{L'} [(P_j^\beta)^\dagger]_{LL'} 4\pi i^{l'} Y_{L'}(\hat{\mathbf{k}}) E_j^0. \quad (4)$$

Here, P_j^β ($\beta = M, N$, $j = x, y, z$) is the transformation matrix which is given in Ref. 20, and is to calculate the j th Cartesian component of the vector spherical waves.²¹ When this plane wave is incident on the sphere, the outgoing waves

from it are generated with its T matrix, t . For the spherical scatterer, the T matrix is decoupled to M and N blocks and is diagonal with L , that is, $t_{LL'}^{\beta\beta'} = \delta_{\beta\beta'} \delta_{LL'} t_L^\beta$. Those outgoing waves will be scattered by the substrate surface. When treating this reflection, the outgoing spherical waves are transformed into the integral of plane waves. The reflection of the plane waves at the plane surface is easily calculated. Then, the reflected plane waves are transformed into the spherical waves, and they act as the incoming waves into the sphere again. This process can be expressed using the matrix $S_{LL'}^{\beta\beta'}$; an incoming wave of $\epsilon_L^{\beta'}$ is scattered by the sphere, then reflected by the substrate, and returns as the incoming waves ϵ_L^β 's with various L 's having the amplitude $S_{LL'}^{\beta\beta'}$. Repeating this process, the amplitudes of all the incoming waves into the sphere, including the incident plane wave and the waves that repeat the scattering between the sphere and substrate surface, are formally written as

$$(1 + St + StSt + \dots) \boldsymbol{\alpha}(0) = (1 - St)^{-1} \boldsymbol{\alpha}(0), \quad (5)$$

where $\boldsymbol{\alpha}(0) = (\dots, \alpha_L^M(0), \dots, \alpha_L^N(0), \dots)^t$. The contribution from the plane wave that is first reflected by the substrate and then is incident on the sphere must be included as well. The details are described by Takemori and co-workers.¹⁷ The difference between theirs and our calculation is the reflection coefficients of the substrate. In Ref. 17 the substrate is a semi-infinite homogeneous material, and the reflection by it is calculated using the Fresnel formulas. In our model, the substrate is covered with the film, so that the reflection coefficients are replaced with the ones for the doubly-layered structure. The sample we consider is the semi-infinite substrate whose dielectric constant is $\bar{\epsilon}_2 \epsilon_0$ covered with the film of thickness d_f and the dielectric constant $\bar{\epsilon}_1 \epsilon_0$. The wave vector of the incoming wave is $(k_x, k_y, -\gamma)$, where $\gamma = \sqrt{k^2 - k_x^2 - k_y^2}$ ($k_y = 0$ for the source \mathbf{j}_p in Fig. 1). When this wave is impinging on the substrate without the sphere, the horizontal component of the wave vector (k_x, k_y) is conserved, and the z component in each region is changed:

$$\gamma_i = \sqrt{\bar{\epsilon}_i k^2 - k_x^2 - k_y^2} \quad (i=1,2). \quad (6)$$

The reflection matrix r_{ij} ($i, j = x, y, z$) is

$$r = \begin{pmatrix} r_s & 0 & r_{xz} \\ 0 & r_s & r_{yz} \\ 0 & 0 & r_p \end{pmatrix}, \quad (7)$$

where r_s and r_p are the reflection amplitudes for the s polarized and p polarized incoming plane waves, respectively; $k = k_1 / \sqrt{\bar{\epsilon}_1} = k_2 / \sqrt{\bar{\epsilon}_2}$ and

$$r_s = \frac{\left(1 - \frac{\gamma_2}{\gamma}\right) \cos \gamma_1 d_f - i \left(\frac{\gamma_2}{\gamma_1} - \frac{\gamma_1}{\gamma}\right) \sin \gamma_1 d_f}{\left(1 + \frac{\gamma_2}{\gamma}\right) \cos \gamma_1 d_f - i \left(\frac{\gamma_2}{\gamma_1} + \frac{\gamma_1}{\gamma}\right) \sin \gamma_1 d_f}, \quad (8)$$

$$r_p = \frac{\left(\frac{k_2^2}{k^2} \frac{\gamma}{\gamma_2} - 1\right) \cos \gamma_1 d_f - i \left(\frac{k_1^2}{k^2} \frac{\gamma}{\gamma_1} - \frac{k_2^2}{k_1^2} \frac{\gamma_1}{\gamma_2}\right) \sin \gamma_1 d_f}{\left(\frac{k_2^2}{k^2} \frac{\gamma}{\gamma_2} + 1\right) \cos \gamma_1 d_f - i \left(\frac{k_1^2}{k^2} \frac{\gamma}{\gamma_1} + \frac{k_2^2}{k_1^2} \frac{\gamma_1}{\gamma_2}\right) \sin \gamma_1 d_f}. \quad (9)$$

r_{xz} and r_{yz} are given by

$$r_{iz} = \frac{-\gamma k_i}{k^2 - \gamma^2} (r_s + r_p) \quad (i=x,y). \quad (10)$$

By this reflection matrix and the procedure expressed by Eq. (5), we can calculate the scattering problem of the system of the sphere above the substrate covered with the film. Since this is an exact solution of the Maxwell equation, the retardation effect is fully included. The z component of the calculated electric field E'_z means the enhancement factor of the field when the plane wave having the amplitude of unity is incident. This plays an important role in calculating the radiation from the STM.⁴ We call this factor G . Using this factor and the reciprocity theorem, the radiated power from the STM gap per unit solid angle becomes

$$\frac{dP}{d\Omega} = \frac{1}{2} \frac{1}{(4\pi)^2 \epsilon_0} \frac{\omega^2}{c^3} |j|^2 |G|^2. \quad (11)$$

Here, the origin of the solid angle Ω is \mathbf{r}_0 . Now we need to estimate the value of $|j|^2$. The form of the point source is $\mathbf{j}(\mathbf{r}) = j \hat{\mathbf{z}} \delta^3(\mathbf{r} - \mathbf{r}_0)$. Since \mathbf{j} is the current density, the unit of j is $[\text{Am}]$. This can be understood as an infinitesimally short and narrow current path $I \cdot \delta l$. From this consideration we put j as Id , where I is the STM current and d is the distance between the sphere and substrate. Although d is finite, $d = 10 \text{ \AA}$, which will be used in the following calculation, may be small enough. Thus $|j|^2$ becomes $I^2 d^2$. The power spectrum $|I_\omega|^2$ of the current fluctuations is defined by

$$|I_\omega|^2 = \sum_f |\langle f | \hat{I} | 0 \rangle|^2 \delta[\omega - (E_f - E_0)/\hbar], \quad (12)$$

where f and 0 label the final and ground states, and \hat{I} is the current operator. The expression for $|I_\omega|^2$ has been evaluated using the tunneling Hamiltonian formalism^{16,22}

$$|I_\omega|^2 = \begin{cases} \frac{eI_0}{2\pi} \left(1 - \frac{\hbar\omega}{eV_b}\right), & 0 < \hbar\omega < eV_b, \\ 0, & eV_b < \hbar\omega, \end{cases} \quad (13)$$

where V_b is the bias voltage between the sphere and substrate. As a result, the radiated power between ω and $\omega + d\omega$ is

$$\frac{dP}{d\Omega} = \frac{1}{2} \frac{1}{(4\pi)^2 \epsilon_0} \frac{\omega^2}{c^3} |G|^2 d^2 |I_\omega|^2 d\omega. \quad (14)$$

If we rewrite this as the radiated power per unit solid angle and photon energy and use Eq. (13), it becomes

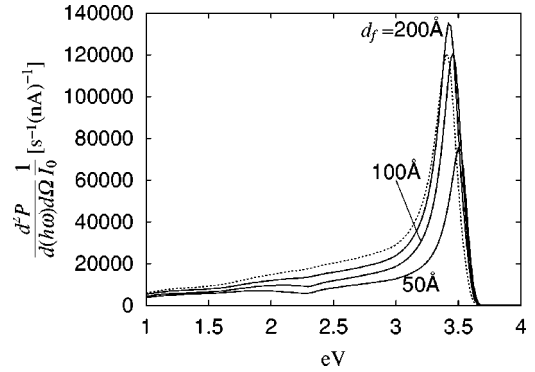


FIG. 2. Radiated power per unit solid angle and photon energy per 1 nA current, for Ag films on the dielectric substrate whose dielectric constant is $\bar{\epsilon}_2 = 11.7$. The dotted line is the plot for $d_f = \infty$. The solid lines are for the Ag films of finite thickness, and its value is varied as $d_f = 200, 100,$ and 50 \AA .

$$\frac{d^2P}{d(\hbar\omega)d\Omega} = \frac{1}{64\pi^3 \epsilon_0} \frac{e}{\hbar c^3} |G|^2 \omega^2 d^2 I_0 \left(1 - \frac{\hbar\omega}{eV_b}\right). \quad (15)$$

The radiated power spectrum will be calculated by using Eq. (15).

III. RESULTS AND DISCUSSION

A. Metal film on a dielectric substrate

We first show the calculation results of the PESTM from a metal film on a dielectric substrate. The sphere (STM tip) is made of W and its radius is $a = 100 \text{ \AA}$. The gap distance between the sphere and the metal surface is $d = 10 \text{ \AA}$. As the dielectric constant of the substrate, we use the value of Si, $\bar{\epsilon}_2 = 11.7$. We make it constant to exclude the optical property of the substrate from a result (the dielectric constant of real Si varies pretty much in the visible range due to direct transitions). The metal film is Ag or Cu. The dielectric functions of these materials are taken from the experimental data of Ref. 23 and that of W is from Ref. 24. The bias voltage between the tip and substrate is $V_b = 4.0 \text{ V}$. Since we employed the current power spectrum as Eq. (13), the current itself becomes a parameter.²⁵ Thus, we have chosen the current as $I_0 = 1 \text{ nA}$. In other words, the calculated radiated power is per 1 nA tunnel current and is proportional to the current value.

The first sample film is Ag. In Fig. 2 we plot the differential radiated power of emitted fields for the different values of film thickness d_f 's. The dotted line is for $d_f = \infty$. The results for $d_f = 200, 100,$ and 50 \AA are plotted by the solid lines. The observation angle is 45° . From this figure, the peak position shows the blueshift as thinning the film. It is notable that the peak height for $d_f = 200 \text{ \AA}$ is about 12% larger than $d_f = \infty$. The peak positions and peak heights for different values of d_f are given in Table I. This indicates the existence of the optimal thickness of the Ag film for the effective light emission, and it may be around $d_f \sim 200 \text{ \AA}$. The peak height for $d_f = \infty$ and $d_f = 100 \text{ \AA}$ is almost the same, but it decreases considerably when $d_f = 50 \text{ \AA}$. The

TABLE I. The peak positions, E_p 's, of the radiated power and the peak height values for various d_f 's of Ag films. Each peak height value is normalized by the value for $d_f = \infty$. The energy step is $\hbar\Delta\omega = 0.02$ eV.

d_f (Å)	E_p (eV)	Height
50	3.50	0.627
100	3.46	1.005
200	3.42	1.123
300	3.42	1.105
400	3.42	1.067
∞	3.40	1

skin depth of Ag in this range of frequencies is about $\delta = 300$ Å so that $d_f = 50$ Å is much smaller than δ . One reason for the decrease of the radiated power is the weaker confinement of electromagnetic fields due to the thinner film, which leads to larger coupling between the localized surface plasmon and the dielectric substrate. Thus, some part of the decreased radiated power may be transmitted into it. This effect becomes clear when d_f becomes less than the skin depth. In this meaning, a thicker film implies the better confinement of electromagnetic fields. Therefore, the existence of the optimal thickness around $d_f \sim 200$ Å is remarkable.

Next we show the results of the Cu film in Fig. 3. It also shows a slight blueshift as thinning the film. The peak height becomes lower with decreasing d_f more rapidly than the Ag film; the curve for $d_f = 200$ Å shows considerable difference with $d_f = \infty$. This is because of the longer skin depth of Cu, which is about $\delta = 700$ Å in the visible range; it is much longer than the film thickness employed in Fig. 3. Thus, the thinning of the film affects the spectra more, and the peak values decrease monotonously. Hence, we cannot find the optimal thickness for the light emission like the Ag film; the spectrum for $d_f = 800$ Å (not shown) is almost the same as that for $d_f = \infty$, and the peak height is lowered gradually by the decrease of d_f .

B. Dielectric film on a metal substrate

In this subsection we consider the effect of a dielectric film covering a metal substrate on the PESTM. Thus, the semi-infinite substrate of dielectric constant $\bar{\epsilon}_2$ is metal, and

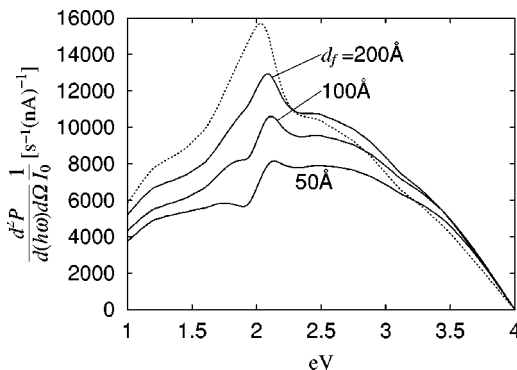


FIG. 3. Same as Fig. 2, but metal films are Cu.

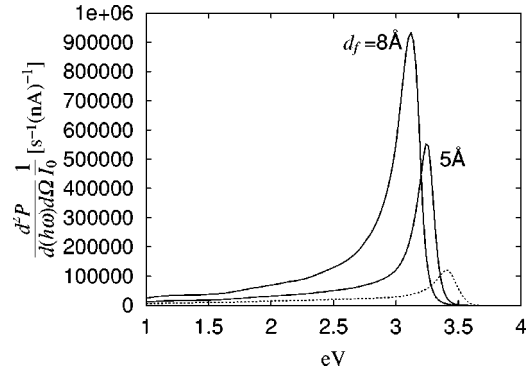


FIG. 4. Two solid lines are the differential radiated power for the Ag substrate covered with dielectric films of different thickness $d_f = 5$ and 8 Å. The dielectric constant of the film is $\bar{\epsilon}_1 = 4$. The dotted curve is for the bare surface ($d_f = 0$).

the film of thickness d_f and dielectric constant $\bar{\epsilon}_1$ is dielectric in this section. In the following calculations, the sphere-metal surface distance is kept constant, $d = 10$ Å, and the thickness of the dielectric film is varied. Therefore, as d_f becomes larger, the sphere-film surface distance becomes shorter.

We use a real dielectric constant for the film, $\bar{\epsilon}_1 = 4$. In Fig. 4 we plot the differential radiated power for two different values of film thickness, $d_f = 5$ and 8 Å by the solid lines. The dotted lines is for the bare surface ($d_f = 0$). It is obvious that the peak value becomes quite larger for the thicker film; when $d_f = 8$ Å the peak is 7.7 times as high as that of the bare surface. One reason for this strong enhancement is the shortening of the air gap which leads to good confinement of electromagnetic field between the sphere and plane surface. Another reason is the enlargement of the enhancement factor $|G|$ by the better electromagnetic coupling between the sphere and metal substrate due to the dielectric film having $\bar{\epsilon}_1 > 1$. The latter reason is supported by the results of varying $\bar{\epsilon}_1$. In Fig. 5, we plot the results of three different dielectric films $\bar{\epsilon}_1 = 2, 3$, and 4 , by the solid lines; the thickness is

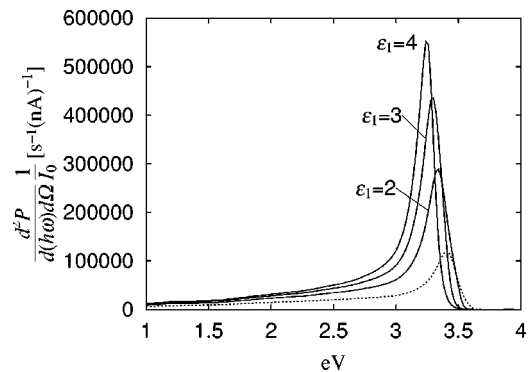


FIG. 5. Differential radiated power for the Ag substrate covered with the dielectric film. The value of the dielectric constant is varied as $\bar{\epsilon}_1 = 2, 3$, and 4 . The film thickness is 5 Å for all three curves. For comparison, the result for the bare surface ($\bar{\epsilon}_1 = 1$) is plotted by the dotted line.

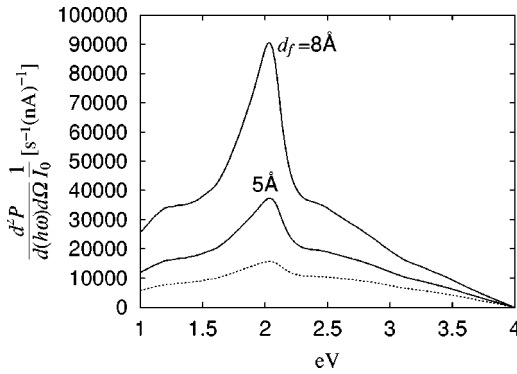


FIG. 6. Same as Fig. 4, but the substrate is Cu.

$d_f = 5 \text{ \AA}$. As $\bar{\epsilon}_1$ becomes smaller, the peak height becomes lower. In both changes, thickening the film and enlarging the dielectric constant, the peak value becomes larger with the redshift. The analysis by Rendell and Scalapino¹⁶ shows that the frequency of the surface plasmon becomes smaller with decreasing the gap distance d . In other words, better coupling between the sphere and substrate leads to the redshift of the peak. The redshift found in the Ag substrate covered with the dielectric film can be understood in a similar way.

We performed the same calculations for the Cu substrate, and the results are in Figs. 6 and 7. With respect to the peak height, a general tendency is very similar to the Ag substrate and the same conclusion can be derived. On the other hand, the redshift is not recognized in the results of the Cu substrate with thickening the film or enlarging $\bar{\epsilon}_1$, however, the peak position is almost unmoved. This may be because Cu is a rather lossy material due to interband transitions and its optical property is quite different from the free-electron-like metal. The peak position of the Cu substrate is pretty affected by the position of the minimum of the imaginary part of the dielectric function.

Although we use the constant current 1 nA for every calculation, this may be changed depending on situations, such as film thickness or dielectric constants. If the current is lowered by thickening the film, the radiated power will be lowered as well. Therefore, we have to estimate the total current and current power spectrum Eq. (13) more precisely when the film is covering the substrate, to make sure that those enhancements really occur in a real experimental condition.

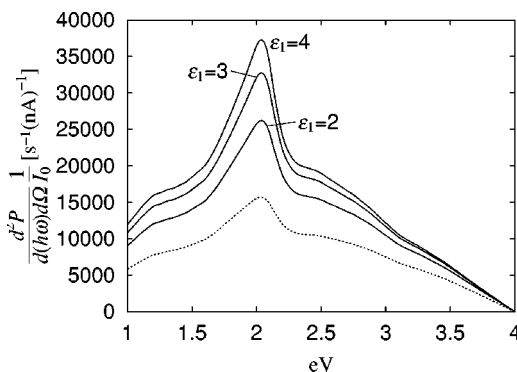


FIG. 7. Same as Fig. 5, but the substrate is Cu.

As a matter of fact, our calculations do not agree very well with reported experimental results. For example, the radiated spectra from the Ag substrate covered with conjugated polymers showed the blueshift from the bare surface spectrum.²⁶ According to another report, the light intensity from the Au film covered with the layer of copper phthalocyanine molecules becomes smaller than that from the uncovered Au film.²⁷ This is also true for the C_{60} -covered Au surface.²⁸ As one of the reasons for these disagreements, those layers is thicker than our model in some data; they could be about 500 Å in Ref. 26. Concerning peak shifts, they should be influenced by the luminescence of molecules themselves. Another possible reason is that the layer of molecules have shown corrugated structures.^{26,27} For the system of the sphere above the substrate, the size of the localized surface plasmon is estimated as $\sqrt{2ad}$ ($d \ll a$).¹⁶ This value is 44.7 Å for our model, and typically less than 100 Å in usual PESTM experiments. Since these values and the corrugation size of molecular layers are of the same order, they may not be treated as homogeneous layers as we modeled. However, we can find some experimental data which agree with our calculations. For example, Fujita and co-workers have shown that the light intensity increased by covering the Cu surface with porphyrin molecules.²⁹ Similar behavior can be seen in the data by Bond and co-workers.²⁶

It must be investigated intensively to what extent our dielectric-film model can be applied to molecular films on metal substrates.

C. Error estimation

In the numerical calculation of the enhancement factor G , we must truncate the basis functions of spherical waves at finite number l_{\max} . We employed $l_{\max} = 20$ for every calculation. For convergence check we compared all the peak values of the enhancement factors with those calculated using $l_{\max} = 25$. For the metal films on the dielectric substrates, the relative error is less than 0.4% for the Ag films, and is less than 0.07% for the Cu films. These values are almost the same as the calculation for the semi-infinite metal substrates. For the calculations of the metal substrates covered with dielectric films, however, the relative error becomes 0.68–4.21% for the Ag substrate and 0.20–1.47% for the Cu substrate. The worst case is $d_f = 8 \text{ \AA}$ ($\bar{\epsilon}_1 = 4$) for both substrates. This is because of the good confinement of the electromagnetic field in the gap region described in Sec. III B. Thus, we may need more bases to calculate the surface plasmon formed there more accurately. Unfortunately, because of the computation time problem, we had to use $l_{\max} = 20$ even for those worst cases. Using our workstation, IBM RS/6000 having Power3 200MHz CPU, it takes about 85 min for one datum point when $l = 20$, and about 220 min when $l = 25$; the required memory space becomes more than twice by this increase of l . The most time-consuming part is the calculation of the matrix elements $S_{LL'}^{\beta\beta'}$. Since the number of bases is $2(l_{\max} + 1)^2$, that of the matrix elements becomes its square and increases rapidly with l_{\max} (the elements to be calculated is much fewer than it because of the symmetry of the model). This is also the reason why the

sphere radius is relatively small; more l must be required for a larger sphere. Truncation around $l_{\max} \sim 40$ would be more appropriate for better accuracy, though much more computational effort would be required. We believe that physical meaning of the calculated results presented here is not changed very much when compared with a more accurate calculation.

IV. CONCLUSIONS

In the present paper we calculated the STM-induced light emission from doubly layered substrates. First, we have shown the results of the metal films on the dielectric substrate. As the film becomes thinner, the peak of the radiated power shows the blueshift. For the Ag film, the optimal thickness for the effective light emission exists. On the other hand, the Cu film shows monotonous decrease of height of the radiation peak with decreasing the film thickness.

The calculation on metal substrates covered with thin dielectric films is also performed. As the film becomes thicker or the dielectric constants of the film become larger, the radiated power is enhanced quite strongly. This is caused in part by the good electromagnetic coupling between the tip and the substrate due to the dielectric film, which leads to the enlargement of the enhancement factor. The redshift of the

peak is observed for the Ag substrate with those changes of the dielectric film, and this may be understood as a shift of the resonance frequency of the localized surface plasmon by the better coupling between the sphere and substrate.

In our calculation we used the current power spectrum derived from the simple metal-insulator-metal model. This may have to be replaced with a more precise model, especially for a metal substrate covered with a dielectric film.

An advantage of our calculation is easiness of treating a multilayered substrate. If its reflection amplitude for the plane wave is known, the radiated power can be calculated. A system of periodically arrayed layers is one example. It is an interesting problem how such a multilayered system changes the nature of the localized surface plasmon and affects the light emission.

ACKNOWLEDGMENTS

We thank D. Fujita for motivating this work. We are grateful to T. Takemori, K. Ohtaka, and H. Miyazaki for valuable discussions. This work was supported in part by the Japanese Ministry of Education, Sports, Culture, Science and Technology through Organized Research Combination System.

-
- ¹J. H. Coombs, J. K. Gimzewski, B. Reihl, J. K. Sass, and R. R. Schlittler, *J. Microsc.* **152**, 325 (1988).
²P. Johansson, R. Monreal, and P. Apell, *Phys. Rev. B* **42**, 9210 (1990).
³R. Berndt, J. K. Gimzewski, and P. Johansson, *Phys. Rev. Lett.* **67**, 3796 (1991).
⁴P. Johansson and R. Monreal, *Z. Phys. B: Condens. Matter* **84**, 269 (1991).
⁵Y. Uehara, Y. Kimura, S. Ushioda, and K. Takeuchi, *Jpn. J. Appl. Phys.* **31**, 2465 (1992).
⁶P. Johansson, *Phys. Rev. B* **58**, 10 823 (1998).
⁷B. N. J. Persson and A. Baratoff, *Phys. Rev. Lett.* **68**, 3224 (1992).
⁸A. Downes, M. E. Taylor, and M. E. Welland, *Phys. Rev. B* **57**, 6706 (1998).
⁹E. Anisimovas and P. Johansson, *Phys. Rev. B* **59**, 5126 (1999).
¹⁰J. Aizpurua, S. P. Apell, and R. Berndt, *Phys. Rev. B* **62**, 2065 (2000).
¹¹A. Madrazo, M. Nieto-Vesperinas, and N. García, *Phys. Rev. B* **53**, 3654 (1996).
¹²I. I. Smolyaninov, M. S. Khaikin, and V. S. Edelman, *Phys. Lett. A* **149**, 410 (1990).
¹³E. Flaxer, O. Sneh, and O. Cheshnovsky, *Science* **262**, 2012 (1993).
¹⁴D. Fujita, T. Ohgi, W.-L. Deng, H. Nejo, T. Okamoto, S. Yokoyama, K. Kamikado, and S. Mashiko, *Surf. Sci.* **454-456**, 1021 (2000).
¹⁵F. Touhari, E. J. A. J. Stoffels, J. W. Gerritsen, and H. van Kempen, *Appl. Phys. Lett.* **79**, 527 (2001).
¹⁶R. W. Rendell and D. J. Scalapino, *Phys. Rev. B* **24**, 3276 (1981).
¹⁷T. Takemori, M. Inoue, and K. Ohtaka, *J. Phys. Soc. Jpn.* **56**, 1587 (1986).
¹⁸J. A. Stratton, *Electromagnetic Theory* (McGraw-Hill, New York, 1941).
¹⁹ Y_L is defined by using the associated Legendre function $P_l^m(\cos \theta)$ of Ferrers' definition as

$$Y_L(\hat{\mathbf{r}}) = (-1)^{(m+|m|)/2} \sqrt{\frac{(2l+1)(l-|m|)!}{4\pi(l+|m|)!}} P_l^{|m|}(\cos \theta) e^{im\phi}.$$

²⁰K. Ohtaka, *Phys. Rev. B* **19**, 5057 (1979).
²¹Because of the different definition of Y_L , the signs of the x and y components of Eqs. (3.2), (3.3), and (3.8) in Ref. 20 should be reversed for our calculation.
²²D. Hone, B. Mühlischlegel, and D. J. Scalapino, *Appl. Phys. Lett.* **33**, 203 (1978).
²³P. B. Johnson and R. W. Christy, *Phys. Rev. B* **6**, 4370 (1972).
²⁴*Handbook of Optical Constants of Solids*, edited by E. P. Palik, (Academic, Orlando, 1985).
²⁵There is a preferable way to determine the total current and current power spectrum, such as the way done in Ref. 4.
²⁶S. F. Bond, A. Howie, and R. H. Friend, *Surf. Sci.* **331-333**, 196 (1995).
²⁷I. I. Smolyaninov, *Surf. Sci.* **364**, 79 (1996).
²⁸R. Berndt, R. Gaisch, J. K. Gimzewski, B. Reihl, R. R. Schlittler, W. D. Schneider, and M. Tschudy, *Science* **262**, 1425 (1993).
²⁹D. Fujita, T. Ohgi, W.-L. Deng, K. Ishige, T. Okamoto, S. Yokoyama, T. Kamikado, and S. Mashiko, *Surf. Sci.* **493**, 702 (2001).